Modeling Microwave Fully Polarimetric Passive Observations of the Sea Surface: A Neural Network Approach

Luca Pulvirenti, *Member, IEEE*, Frank Silvio Marzano, *Senior Member, IEEE*, and Nazzareno Pierdicca, *Member, IEEE*

***Abstract*—The two-scale electromagnetic model is a well-established theory for simulating microwave polarimetric passive observations of a sea surface. A critical aspect is the long computational time that is required to run the forward model, which hampers the creation of large training databases or iterative simulations within retrieval algorithms. To tackle this problem, a neural network (NN) technique is proposed in this paper. In particular, we have adopted NNs to emulate a simulator named SEAWIND, which implements the two-scale model and was validated in previous works. Two training algorithms, including a regularized approach, have been considered and compared. The assessment of the proposed approach has been carried out by statistically comparing neural-network-derived simulations with SEAWIND-derived ones for two validation data sets comprising different climatic conditions, as well as by computing the azimuthal Fourier harmonic coefficients versus wind speed and atmospheric transmittance. Regressive model functions have also been used as benchmarks. This paper demonstrates the feasibility of an NN approach to efficient and effective modeling of sea-surface thermal emission and scattering.**

***Index Terms*—Microwave radiometry, neural network (NN), polarimetry, satellite passive remote sensing, scattering model, sea surface.**

I. Introduction

GLOBAL monitoring of both wind speed and direction (hereinafter also called wind vector) has been mainly performed by means of satellite active microwave scatterometers until recently. In the last decade, several aircraft experiments have demonstrated that polarimetric microwave radiometric observations are sensitive to the wind vector as well (e.g., [1] and [2]). The WindSat fully polarimetric radiometer [3], which was launched in 2003 aboard the Coriolis satellite, currently continuously supplies polarimetric passive measurements. The WindSat radiometer represents a complementary sensor to scatterometers, with the additional capability of retrieving further sea and atmospheric variables that are typically derived from spaceborne microwave radiometric measurements.

Manuscript received May 18, 2006; revised February 9, 2007.

L. Pulvirenti and N. Pierdicca are with the Department of Electronic Engineering, University of Rome "La Sapienza," 00184 Rome, Italy (e-mail: pulvirenti@die.uniroma1.it; pierdicca@die.uniroma1.it).

F. S. Marzano is with the Department of Electronic Engineering, University of Rome "La Sapienza," 00184 Rome, Italy, and also with the Center of Excellence CETEMPS, University of L'Aquila, 67100 L'Aquila, Italy (e-mail: marzano@die.uniroma1.it).

Digital Object Identifier 10.1109/TGRS.2007.897447

Modeling the polarimetric microwave signature of the sea-surface emission is essential for wind vector retrieval. Several electromagnetic theories are available in the literature, which are generally derived from scattering models through the application of the polarimetric Kirchoff's law. Among them, the two-scale model (TSM) [4]–[6] is fairly popular and widely adopted to generate synthetic satellite passive polarimetric observations, i.e., to simulate the modified Stokes' vector $\mathbf{T}_B$, whose components are the brightness temperatures at vertical (T_{Bv}) and horizontal (T_{Bh}) polarizations, and correlation parameters U and V, which are emitted and scattered by a marine surface.

In previous works, we have developed and validated a software package named SEAWIND [7]–[9] within a joint project that was funded by the European Space Agency. SEAWIND implements the TSM based on the work of Yueh [4] and includes a radiative transfer scheme to account for the atmospheric effects, thus simulating $\mathbf{T}_B$ at the top of the atmosphere. The shortcoming of SEAWIND, as well as of any other simulator that is based on the two-scale approach, is its long computational time. The calculation of a single Stokes' emissivity vector (related to $\mathbf{T}_B$, as it will be clear in Section II) for a given state of the sea–atmosphere system, i.e., for specified values of the environmental variables (sea-surface temperature, wind speed and direction, atmospheric transmittance, etc.), involves the evaluation of two double integrals.

The low computational efficiency of the TSM makes its use difficult in generating large data sets of simulations that are required to train retrieval algorithms, as well as exploiting iterative techniques to solve the inverse problem. The improvement of the efficiency of the two-scale approach represents therefore a crucial aspect. This problem has been tackled by Lyzenga and Vesecky [10] by expanding the azimuthal dependence of the local emissivity in a Fourier series (up to second order) and analytically evaluating one of the two double integrals after an expansion of the integrand in a Taylor series. Johnson [11] noted that, in [10], the atmospheric effects have not been taken into account (they have been considered by Lyzenga in [12]). In [11], an efficient implementation of the TSM based on a tabling of repeated calculations and on the use of Taylor series expansions has been carried out, and the atmosphere has been accounted for.

An alternative way to deal with the problem of improving the TSM computational efficiency is to resort to a multilayer feed-forward neural network (NN). The latter one, having at least one hidden layer, can approximate any nonlinear function

relating inputs to outputs [13] and can be adopted to emulate a forward electromagnetic model giving advantages in terms of computational speed and maintaining a fairly good degree of accuracy. The adoption of an NN technique to improve the efficiency of oceanic models has already been proposed by Krasnopolsky *et al.* [14]. In their study, they have successfully applied such a technique for approximating the UNESCO equation of state to compute sea water density or salinity.

In this paper, our aim is to develop an NN that is able to reproduce the behavior of the SEAWIND simulator, thus modeling microwave fully polarimetric observations of a sea surface. To do this, a training set consisting of matched pairs of vectors of geophysical parameters and satellite synthetic data, which are formed by pairs of SEAWIND inputs and outputs ($\mathbf{T}_B$'s), has been built. Individual NNs have been designed for each of the three WindSat polarimetric frequencies. The validation of the NN approach has been accomplished by comparing the SEAWIND outputs with the NN ones. A standard approach, which is based on regressive model functions (RMFs), has also been considered as a benchmark. It is worth noticing that NNs do not require any analytical assumption about the model that they need to approximate since they learn from the examples that are included in the training set [15]. Conversely, the use of RMFs implies prior selection of their functional form.

This paper is organized as follows. In Section II, a summary of the two-scale model that is implemented in the SEAWIND simulator is provided. Section III introduces the algorithms that are adopted to train the networks and describes the design of the NN architecture. In Section IV, the NN-derived simulations of the modified Stokes' vector are assessed against SEAWIND outputs and RMF-derived ones. Furthermore, an evaluation of the impact on wind speed retrieval of the discrepancies between SEAWIND and its NN emulator is furnished.

II. Two-Scale Polarimetric Model of Sea Emission

The SEAWIND software package implements the TSM formulation that was proposed by Yueh [4] to compute the surface polarimetric emission and accounts for the atmospheric contribution (i.e., both upward atmospheric unpolarized emission and downward emission scattered by the surface) according to Pierdicca *et al.* [8]. SEAWIND computes the modified Stokes' vector $\mathbf{T}_B$, which is observed at the satellite altitude. The U and V components of $\mathbf{T}_B$ are originated by the anisotropic shape of the wind-induced sea waves, acting as emission source and scattering the impinging atmospheric radiation.

The two-scale model assumes that the sea surface is composed of a small wavelength roughness that is superimposed on large-scale waves. The wavenumber that separates the two roughness scales is a function of the electromagnetic wavelength. From one side, it is such that the large waves can be considered as plane patches with dimensions of several electromagnetic wavelengths. On the other side, the electromagnetic scattering due to the residual spectrum of small-scale roughness should be interpreted by the small perturbation method (SPM) [16], [17]. Therefore, the brightness temperature vector at the sea surface (i.e., at the bottom of the atmosphere, BOA) $\mathbf{T}_{\mathrm{BOA}}$ in a direction θ, φ is due to the incoherent summation of the brightness temperature of each tilted rough patch $\mathbf{T}_{\mathrm{SEA}}$ and is obtained by averaging over the probability density function (pdf) $P(S_x, S_y)$ of the slope of the patches (assumed Gaussian) in the upwind S_x and crosswind S_y directions, i.e.,

$$\mathbf{T}_{\mathrm{BOA}}(\theta,\varphi)=\int_{-\infty}^{+\infty} dS_y \int_{-\infty}^{+\cot\theta} \mathbf{T}_{\mathrm{SEA}}(1-S_x\tan\theta)P(S_x,S_y)dS_x. \tag{1}$$

In (1) and in the rest of this section, the dependence on frequency is assumed to be implicit.

SEAWIND adopts the sea water permittivity model that was developed by Ellison *et al.* [18] and foam emissivity ε_f that was proposed by Pandey and Kakar [19], while for foam fraction F, the formula that was given by Wilheit [20] has been selected. Brightness temperature vector $\mathbf{T}_{\mathrm{SEA}}$ partially (i.e., fraction $1-F$) originates from the thermal emission of the anisotropic roughness that is induced by the wind stress plus its scattering of incident unpolarized brightness temperature T_{IN} (i.e., that emitted downward by the atmosphere plus a small contribution of the cosmic background attenuated by the atmosphere). Fraction F of $\mathbf{T}_{\mathrm{SEA}}$ is determined by ε_f plus the foam scattering, which is assumed specular with an equivalent reflectivity equal to $(1-\varepsilon_f)$. Consequently, $\mathbf{T}_{\mathrm{SEA}}$ is given by

$$\mathbf{T}_{\mathrm{SEA}}(\theta,\varphi) = (1-F)\mathbf{T}_R(\theta,\varphi) + F\varepsilon_f T_s\mathbf{I} + F(1-\varepsilon_f)T_{\mathrm{IN}}\mathbf{I} \tag{2}$$

where $\mathbf{T}_R$ originates from the wind-roughened surface without foam, and T_s is the surface physical temperature. $\mathbf{I}$ is a 4×1 vector whose first two components are equal to 1, while the others are equal to 0. Note that (2) implies that foam emission has third and fourth Stokes' parameters equal to zero. This simplification is due to the fact that commonly adopted foam models (e.g., [19]) provide only the emissivity at horizontal and vertical polarizations. $\mathbf{T}_R$ is found by using the generalized Kirchhoff's law to express the Stokes' emissivity vector $\boldsymbol{\varepsilon}$ and adding incoherently brightness temperature vector $\mathbf{T}_{\mathrm{SC}}$ that is scattered by the rough surface, i.e.,

$$\begin{aligned}\mathbf{T}_R(\theta,\varphi) &= T_s\boldsymbol{\varepsilon}(\theta,\varphi) + \mathbf{T}_{\mathrm{SC}}(\theta,\varphi)\\ &= T_s\left\{\mathbf{I} - \frac{1}{4\pi}\int_0^{\pi/2}\sin\theta_i d\theta_i \int_0^{2\pi} d\varphi_i \mathbf{g}\right\}\\ &\quad + \frac{1}{4\pi}\int_0^{\pi/2}\sin\theta_i d\theta_i \int_0^{2\pi} d\varphi_i T_{\mathrm{IN}}\mathbf{g}\end{aligned} \tag{3}$$

where the double integrals are extended to all possible incident directions θ_i, φ_i, and $\mathbf{g}$ is a 4×1 vector, whose components depend on the bistatic scattering coefficients that are given by the second-order SPM. They are related to the anisotropic power spectrum of the sea waves in the gravity-capillary wavenumber range, where SPM is applicable.

The last step for computing the modified Stokes' vector $\mathbf{T}_B$ that is observed by a satellite radiometer consists of making explicit the effects of the atmosphere. Assuming that the atmosphere is plane parallel and the scattering source function can be neglected (i.e., rain effects are not considered), if γ denotes the atmospheric transmittance for a slant path ($\gamma = e^{-\tau/\cos\theta}$, where τ indicates the optical thickness) and T_{UP} represents the upwelling atmospheric brightness temperature, we can express $\mathbf{T}_B$ as

$$\begin{aligned}\mathbf{T}_B(\theta,\varphi) &= \mathbf{T}_{\mathrm{BOA}}(\theta,\varphi)\gamma + T_{\mathrm{UP}}\mathbf{I} \\ &= \mathbf{T}_{\mathrm{BOA}}(\theta,\varphi)\gamma + T_{\mathrm{mrup}}(1-\gamma)\mathbf{I} \end{aligned} \tag{4}$$

where T_{mrup} is the upwelling mean radiative temperature. In this case, T_{IN} is given by

$$T_{\mathrm{IN}} = T_{\cos}\gamma + T_{\mathrm{DN}} = T_{\cos}\gamma + T_{\mathrm{mrdn}}(1-\gamma) \tag{5}$$

where T_{DN} is the downwelling atmospheric brightness temperature, $T_{\cos}$ is the cosmic background (assumed equal to 2.7 K), and T_{mrdn} is the downwelling mean radiative temperature.

The azimuthal dependence and the amplitude of the U and V components are the fundamental quantities that allow one to derive both wind intensity and wind direction from polarimetric radiometry. Consequently, the modeling of the surface azimuthal anisotropy is an essential aspect of the simulations. In the SEAWIND package, there are two main geophysical factors determining such anisotropy: 1) the anisotropy of the sea wave spectrum (spreading function), which determines the asymmetry between downwind and crosswind observations of the radiometer, and 2) the hydrodynamic modulation, which accounts for the upwind to downwind asymmetry. To describe such anisotropic behavior, the sea wave spectrum that was developed by Durden and Vesecky [21] and the hydrodynamic modulation that was proposed by Yueh [4] have been implemented in the SEAWIND software package. With respect to [21], the value of the absolute magnitude of the amplitude spectrum is equal to 0.007, instead of 0.004. This modification has permitted us to well reproduce the radiometric measurements for a midlatitude environment, such as the Mediterranean basin [9].

III. Neural-Network Approach to Forward Modeling

An artificial NN is a nonlinear parameterized mapping from an input vector $\mathbf{x}$ to an output vector $\mathbf{y} = NN(\mathbf{x};\mathbf{w},M)$, where $\mathbf{w}$ is the weight vector (including the biases as well) and M is the architectural model of the network. The multilayer perceptron (MLP) architecture considered here is a mapping model that is composed of several layers of parallel processors (i.e., neurons). It has been theoretically proven that one-hidden-layer MLP network may represent any continuous function [22], while a two-hidden-layer MLP may approximate any function to any degree of nonlinearity, taking also into account discontinuities [23]. NNs have a large variety of applications in passive and active remote sensing, which are mainly devoted to retrieval purposes (e.g., [14] and [24]).

A. NN Training Algorithms

The NN architecture is such that all nodes are fully interconnected to each other, and this interconnection is characterized by weights and biases. We can distinguish the hidden weights w_{km}, i.e., the weight of the kth hidden node that is associated with the mth input value, from the output weights w_{jk}, i.e., the weight of the jth output node that is associated with the kth hidden value. Biases, which are initialized to 1, are input to both the hidden and output layers. The hidden and output nodes are characterized by an activation function f_{act}, which is generally assumed to be a differentiable nonlinear function. Here, we have chosen the sigmoidal (logistic) function *tan-sigmoid*, which is characterized by the node gain and the node bias.

The network is trained by supervised learning using training data set $D = \{\mathbf{x}(i),\mathbf{t}(i)\}$, which consists of available inputs $\mathbf{x}(i)$ and desired targets $\mathbf{t}(i)$, where $i = 1 : N_r$ and N_r is the number of training-coupled patterns (e.g., records). During training, the weights and biases are iteratively adjusted in order to minimize the network performance or objective function (error correction learning), which normally is the sum of squared errors E_D, i.e.,

$$E_D(\mathbf{w}) = \sum_{i=1}^{N_r} [\mathbf{t}(i) - \mathbf{y}(i)]^T [\mathbf{t}(i) - \mathbf{y}(i)] \tag{6}$$

where $\mathbf{y}(i)$ is the NN response to the ith input pattern, and superscript "T" indicates matrix transpose. The minimization with respect to $\mathbf{w}$ is based on repeated evaluation of the gradient of the performance function using the backpropagation algorithm, which involves performing computations backward through the network [25]. The backpropagation learning rule can be implemented by using a steepest gradient descent algorithm. However, in this paper, the optimization problem has been solved by using the Levenberg–Marquardt (LM) algorithm, which has proven to be highly efficient and able to provide the error Hessian matrix useful for further analyses, as will be clear subsequently [26]. The NN that is trained by the LM algorithm has been named as LMNN.

The ideal NN is characterized by small errors on the training set and the capability to respond properly to new or erroneous inputs. The latter NN property is called generalization. The procedure to improve generalization, which is called regularization, usually adds an additional term to the error objective function, which becomes E_R, i.e.,

$$E_R(\mathbf{w}) = \alpha_D E_D(\mathbf{w}) + \alpha_W E_W(\mathbf{w}) \tag{7}$$

where E_W is the sum of the squares of the network weights $\mathbf{w}$ (i.e., $\Sigma_i \mathbf{w}^{\mathrm{T}}\mathbf{w}$), while α_D and α_W are the regularization parameters. If $\alpha_D \gg \alpha_W$, the training algorithm will minimize the NN error term E_D, while if $\alpha_D \ll \alpha_W$, the algorithm will emphasize weight size reduction, at the expense of larger network errors, producing a smoother but more robust network response. In other words, the regularized NN tends less likely to overfit the training data points. It has been experimentally proven that, for noisy data, a one-hidden-layer MLP network

may improve the network generalization through the reduction of the number of neurons [27].

A critical issue when dealing with (7) is to set the optimal values for regularization parameters α_D and α_W. Heuristic approaches may be followed, but an automatic and rigorous procedure should be preferred. A way to approach this problem is to resort to the Bayesian theory, where weights $\mathbf{w}$ are considered as random variables [28]. The estimation procedure is formally quite complex, and here, we briefly summarize it, referring to [28] and [26] for further details.

The posterior pdf $p(\mathbf{w}|D, M, \alpha_D, \alpha_W)$ of $\mathbf{w}$ can be calculated by assuming a Gaussian pdf for the training data set errors and for the prior pdf of $\mathbf{w}$. Under these hypotheses, maximizing $p(\mathbf{w}|D, M, \alpha_D, \alpha_W)$ with respect to $\mathbf{w}$ becomes equivalent to minimizing the regularized error function $E_R(\mathbf{w})$. The regularization parameters α_D and α_W, which are supposed to be uniformly distributed, are then estimated by maximizing their posterior probability $p(\alpha_D, \alpha_W|D, M)$, which, in turn, can be explicitly related to $p(\mathbf{w}|D, M, \alpha_D, \alpha_W)$ by means of Bayes' rule [28] and to a proper normalization function of α_D and α_W. The latter one can be approximated by expanding the regularized error function $E_R(\mathbf{w})$ by means of a Taylor series up to the second order around the minimum point $\mathbf{w}_0$ (where the gradient of E_R is zero). Finally, the optimal values of α_D and α_W can be explicitly calculated as stationary points of $p(\alpha_D, \alpha_W|D, M)$, and the result is [28]

$$\hat{\alpha}_D = \frac{n_w - n_e}{2E_D(\mathbf{w}_0)} \quad \hat{\alpha}_W = \frac{n_e}{2E_W(\mathbf{w}_0)} \tag{8}$$

where n_w and n_e are the total and effective numbers of NN weights, respectively. The latter one is $n_e = n_w - 2\alpha_W \mathrm{tr}[\mathbf{H}(\mathbf{w}_0)]$, where tr is the matrix trace and $\mathbf{H}$ is the Hessian matrix of $E_R(\mathbf{w}_0)$ (i.e., $\nabla^2 E_R$) that is evaluated through the Gauss–Newton approximation, using the Jacobian matrix $\mathbf{J}$ of E_D, and is directly available within the LM algorithm [26].

The initialization values of α_D and α_W are usually 1 and 0, respectively. After having initialized $\mathbf{w}$ by means of random generation and having normalized the training data set to [−1,1], the Bayesian-regularized NN (BRNN) training algorithm: 1) minimizes E_R by finding $\mathbf{w}_0$ using the LM technique; 2) computes n_e by approximating $\mathbf{H}(\mathbf{w}_0)$; 3) estimates α_D and α_W through (8); and 4) iterates until the change of E_R between two successive iterations is below a given threshold, so that the convergence is ensured. Note that, at each iteration (epoch), both the error objective function E_R and minimum point $\mathbf{w}_0$ of E_R are changed.

B. Design of Forward Model NN

The training databases for developing the NN span the three WindSat polarimetric frequency channels $f_i (i = 1:3;$ $f_1 = 10.7, f_2 = 18.7, f_3 = 37.0$ GHz) at the corresponding incidence angles (49.9°, 55.3°, and 53.0°, respectively). They have been formed by $3 \times N_r$ runs of the SEAWIND simulator, where N_r is the number of runs for each band. As input variables, we have considered the following: the azimuth angle between wind and radiometer pointing directions φ, wind friction velocity u^*, sea-surface temperature T_s, atmosphere optical thickness τ, and mean radiative temperatures T_{mrdn} and T_{mrup}. Other parameters, such as sea water salinity (S), have been considered as constants ($S = 35$ ppm has been assumed). In practice, the training set is formed by N_r records. Each record includes 24 variables, i.e., 12 inputs: φ, u_*, T_s, $\tau(f_i)$, $T_{\mathrm{mrdn}}(f_i)$, and $T_{\mathrm{mrup}}(f_i)$, and 12 SEAWIND outputs: $T_{\mathrm{Bv}}(f_i)$, $T_{\mathrm{Bh}}(f_i)$, $U(f_i)$, and $V(f_i)$.

The values of the input variables (predictors) belonging to the training set have been randomly generated. The azimuth angle has been supposed to be uniformly distributed between 0° and 360°. The wind friction velocity has been derived from the wind speed at 19.5 m above sea level (u_{19}) by fitting the relationship that is given in [4]. For the latter one, we have assumed a truncated (to discard negative values) Gaussian distribution that is characterized by a mean value equal to 5 m/s and by a standard deviation equal to 2.5 m/s. As for T_s, it has been considered to be uniformly distributed between 10 °C and 27 °C. The mean radiative temperatures have also been supposed to be uniform. T_{mrdn} has been assumed to be in the range of 262–279 K at 10 GHz, 269–287 K at 18 GHz, and 265–285 K at 37 GHz. A linear relationship between T_{mrup} and T_{mrdn} has been considered since they derive from the integration of slightly different functions depending on the same profile of atmospheric parameters, and their correlation coefficient is very high. A Gaussian distribution has been adopted for the optical thickness, with the following mean values (hereinafter denoted by m_τ) and standard deviations (hereinafter indicated by σ_τ): $m_\tau(f_1) = 0.015$, $\sigma_\tau(f_1) = 0.003$, $m_\tau(f_2) = 0.060$, $\sigma_\tau(f_2) = 0.015$, $m_\tau(f_3) = 0.090$, and $\sigma_\tau(f_3) = 0.025$. It is worth noting that we have selected the statistics of the predictors by referring to typical conditions of a midlatitude region (for which SEAWIND has been assessed in [9]) without precipitation. Although the choice of both the distributions and the dynamic range of the input variables may be questioned, it does not represent a very critical point due to the generalization ability of the NNs and, particularly, of the BRNN.

After having generated the training database, the actual network design has been carried out. We have built identical NN architectures for the three radiometric frequencies and for both the training algorithms that we have used. Each architecture consists of five input neurons (corresponding to φ, u_*, T_s, τ, and T_{mrdn}), one hidden layer of N_h neurons, and four output neurons (corresponding to the four components of the modified Stokes' vector). Notice that T_{mrup} has been excluded from the set of NN inputs since, in the training database, we have assumed a linear relationship with T_{mrdn}. Only one layer of hidden neurons has been used, taking advantage of the capability of this kind of network to approximate any continuous function, as already mentioned. By monitoring the objective function, we have found that a number of learning cycles (epochs) that is equal to 200 ensures its minimization for both learning methods.

To select the numbers of hidden neurons N_h and required records of the training set N_r, the sensitivity of the NN accuracy to these parameters has been evaluated. To do this, we have

TABLE I
rmse_{TOT} COMPUTED FOR DIFFERENT VALUES OF N_r AND N_h

	N_r=250	N_r=500	N_r=1000	N_r=2000
N_h = 10	0.71	0.52	0.41	0.40
N_h =15	0.35	0.27	0.25	0.25
N_h =20	0.21	0.19	0.17	0.16
N_h =25	0.23	0.18	0.17	0.15

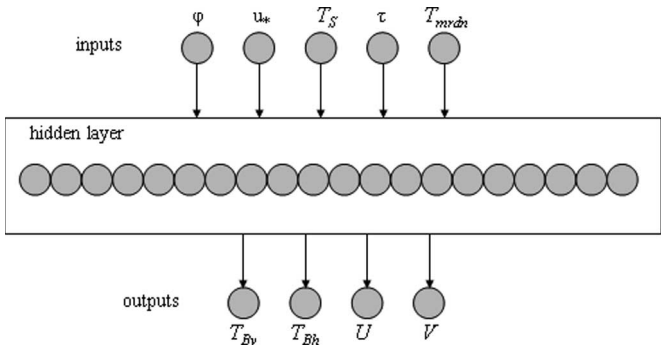

Fig. 1. NN architecture including the inputs, one hidden layer of 20 neurons, and the outputs.

considered one of the validation data sets that we have built (DB1, see Section IV), we have compared the SEAWIND outputs with the NN ones, and we have expressed the results in terms of total root mean square error (rmse_{TOT}), which is defined, for a given frequency, as

$$\text{rmse}_{\text{TOT}} = \sqrt{\sum_{q=1}^{4} \text{rmse}_q^2} \tag{9}$$

where rmse_q is the root mean square error for the qth component ($q = 1:4$) of $\mathbf{T}_B$, which is denoted by T_{Bq} with $T_{B1} = T_{\text{Bv}}$, $T_{B2} = T_{\text{Bh}}$, $T_{B3} = U$, and $T_{B4} = V$. For a given value of N_r (250, 500, 1000, 2000), we have computed rmse_{TOT} for different N_h's (from 10 to 25 with step 5).

Table I reports the results of the sensitivity analysis. For the sake of conciseness, only the 37-GHz channels and BRNN (the network that yields the best performance, as will be shown in Section IV) are considered. From Table I, it can be observed that rmse_{TOT} rapidly decreases with increase of N_h from 10 to 20, for each value of N_r, while it tends to become more stable for $N_h \geq 20$. Moreover, for every N_h, the augmentation of N_r from 1000 to 2000 implies a slight improvement of the performances of BRNN and a considerable increase of the time that is required to train the network. We have therefore chosen 20 neurons for the hidden layer and $N_r = 1000$ records, having considered that this is good compromise between accuracy of the results and complexity of the architecture.

Fig. 1 illustrates the architecture of the adopted NNs. Since the activation function f_{act} of the hidden neurons is a *tan-sigmoid* and that of the output neurons is linear, such architecture implies that the NN outputs can be expressed by the following relationship:

$$T_{Bq} = \sum_{j=1}^{20} \omega_{qj} \left[\tan\text{sig} \left(\sum_{i=1}^{5} w_{ji} x_i + bj \right) \right] + \beta_q, \qquad q = 1:4 \tag{10}$$

where w_{ji} and b_j represent the weights and biases of the jth neuron of the hidden layer ($j = 1:20$); ω_{qj} and β_q denote the weights and biases of the qth neuron of the output layer, respectively; and the generic input variable is indicated by $x_i (i = 1:5)$.

Obviously, the weights and biases depend on the adopted backpropagation training algorithm. In [29], an example, reporting the values of w_{ji}, b_j, ω_{qj}, and β_q for the network that is trained with the Bayesian regularization method for the 37-GHz channels, is explicitly given.

IV. NN APPROACH ASSESSMENT

The last step of our study has consisted of the assessment of the proposed approach. It has been basically performed by comparing the $\mathbf{T}_B$'s that are produced by the different simulators that we have considered (SEAWIND, NNs, and RMFs). Furthermore, an estimate of the impact of the errors on wind-speed retrievals due to the application of the NN forward model, as opposed to the explicit electromagnetic model, has been attempted. It should be stressed that, in this paper, we rely on the simulation performance of the TSM and on its implementation in SEAWIND, whose validation is beyond the scope of this paper. Although many papers have proven the reliability of TSM (e.g., [4]), the first WindSat observations of the V signal at 37 GHz are actually much weaker with respect to those predicted by TSM [30]. Yueh *et al.* [30] suppose that this may be due to deficiencies in the two-scale ocean model. From our point of view, in the event an updating of the electromagnetic model will become necessary, the procedure that is described before (generation of training set, NN architecture, and its optimization) can be rerun in a straightforward way. In fact, future changes of TSM are not expected to produce very different radiometric signatures but only to better reproduce sensitivity of V to geophysical parameters, so that the change in terms of NN structure is not expected to be very significant.

A. Validation Databases

Although the approximation accuracy of the NNs is monitored during the training phase (through the evaluation of the objective function), a major issue is the capability of the training set to really represent the space of possible input parameters or, in other words, the capability of the NNs to correctly respond to inputs that are not well represented in the training set. We have considered validation sets that are completely different from the training one in order to evaluate the generalization ability of the network.

The first validation database (hereinafter named as DB1) has been derived from a set of meteorological analyses that have been supplied by the European Centre for Medium-Range Weather Forecasts (ECMWF) and have been collected throughout the first ten days of each month of year 2000 over the Mediterranean Sea. From such analyses, we have extracted the vertical profiles of temperature, pressure, and relative humidity, as well as the surface value of sea temperature and wind velocity. We have then applied a radiative transfer algorithm in a nonscattering atmosphere to compute τ, T_{mrdn}, and T_{mrup}

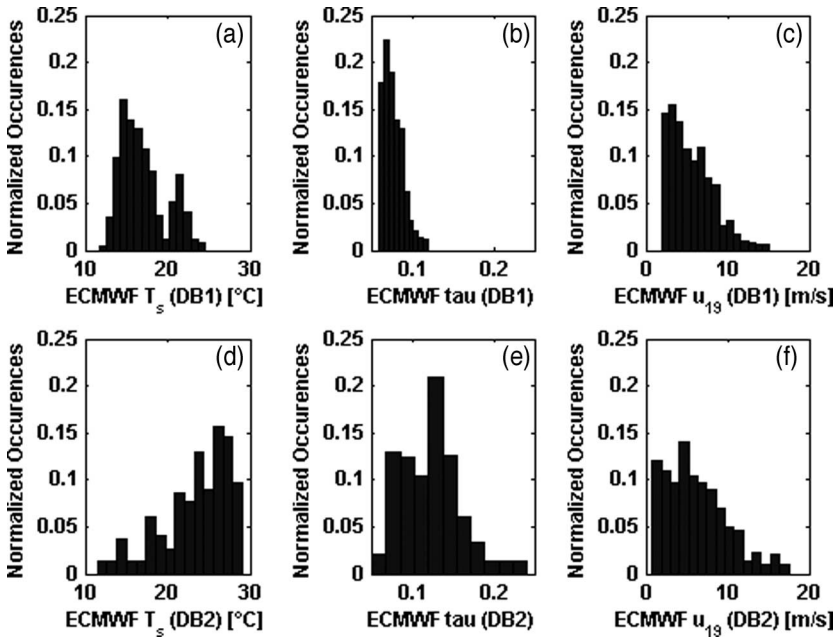

Fig. 2. Statistics of (a) and (d) T_s, (b) and (e) τ, and (c) and (f) u_{19} for DB1 (Mediterranean Sea, upper panels) and DB2 (Open Ocean, bottom panels).

[9]. Parameter φ originates from the combination of wind direction and sensor look direction, and since in this paper the radiometric data are simulated, we have decided to still generate φ randomly but independently from the training set.

A second validation database (hereinafter named as DB2) has been derived from a set of ECMWF meteorological profiles concerning the open ocean, specifically, the North Atlantic and the South Atlantic. This set has been acquired in the framework of the passive calibration activity of the radar altimeter onboard Envisat [31]. The use of DB1 and DB2 aims to have two validation databases that are related to different climatic and surface conditions for the purpose of verifying the ability of the network to reproduce the behavior of the SEAWIND in the presence of different sets of inputs.

Fig. 2 compares the statistics of DB1 and DB2 for three variables: 1) T_s; 2) τ at 37 GHz; and 3) wind speed u_{19}, which is closely related to u_*. By examining this figure, the considerable differences for τ and T_s clearly emerge. These differences could be due to the fact that the humidity of an oceanic environment is higher than that of a closed basin, such as the Mediterranean Sea.

B. RMFs

Another approach to overcome the difficulties of using detailed electromagnetic models consists of introducing RMFs (e.g., [30] and [32]). They are usually based on statistical regression analyses of training sets that are derived from actual measurements or an electromagnetic model. Since we are interested in comparing the performances of the forward NN with the RMF approach, a set of RMFs has been derived from the same training set that is produced by SEAWIND to train the NN, but making reference to functional forms that are already proposed in the literature. The components of $\mathbf{T}_B$ can be approximately written as (11a) and (11b), shown at the bottom of the page [33], [34].

As mentioned, $q = 1, 2$ refers to T_{Bv} and T_{Bh}, respectively, while $q = 3, 4$ refers to U and V, respectively. The surface emissivity for the qth component is denoted by ε_q, while the term Ω represents a correction factor that accounts for nonspecular reflection. For $q = 1, 2$, we have chosen the expression of Ω that is given in [32], while for $q = 3, 4$, we have carried out a linear fit of the values of Ω that are provided by [34] for wind speeds equal to 8 and 16 m/s. From each $\mathbf{T}_B$ simulation belonging to the training set, we have derived the corresponding emissivity vector $\boldsymbol{\varepsilon}$ by means of (11). Then, we have expanded the components of $\boldsymbol{\varepsilon}$ in harmonics [34] as in

$$\varepsilon_q = \begin{cases} a_{0q} + a_{1q}\cos\varphi + a_{2q}\cos 2\varphi, & q = 1, 2 \quad (12a) \\ d_{0q} + d_{1q}\sin\varphi + d_{2q}\sin 2\varphi, & q = 3, 4 \quad (12b) \end{cases}$$

where a_{iq} and d_{iq} are the coefficients $(i = 0 : 2)$. It is worth noting that d_{0q} is generally thought to be zero (for $q = 3, 4$) and is included in (12b) only to account for possible offsets [34]. The coefficients a_{0q} have been expressed as in [9], while for $a_{1q,2q}$, the form that is proposed in [32] has been used.

$$T_{Bq} = \begin{cases} T_{\mathrm{UP}} + \gamma\left[\varepsilon_q T_s + (1-\varepsilon_q)(\Omega T_{\mathrm{DN}} + \gamma T_{\cos})\right], & q = 1, 2 \quad (11a) \\ \gamma\varepsilon_q\left[T_s - (\Omega T_{\mathrm{DN}} + \gamma T_{\cos})\right], & q = 3, 4 \quad (11b) \end{cases}$$

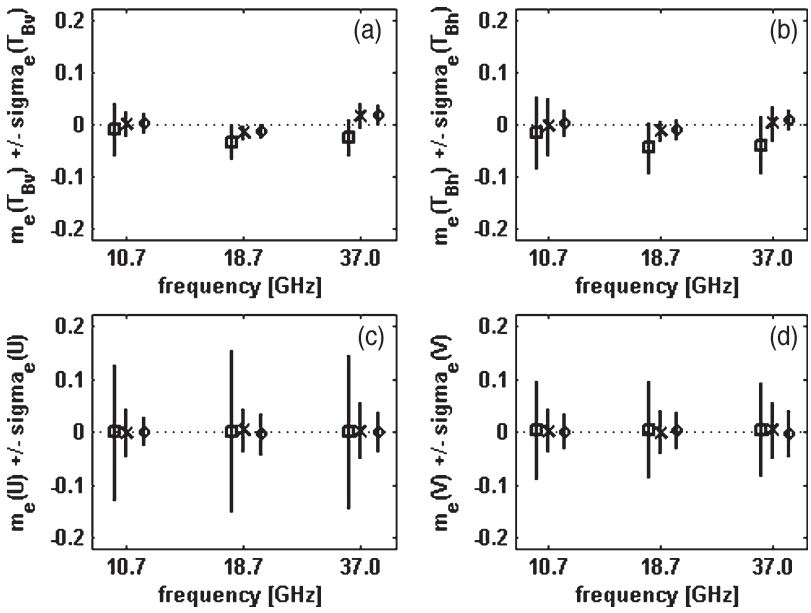

Fig. 3. $m_e \pm \sigma_e$ (sigma$_e$) for (a) T_{Bv}, (b) T_{Bh}, (c) U, and (d) V. m_e is indicated by squares (RMFs), crosses (LMNN), and circles (BRNN). σ_e is represented by solid lines. DB1 (Mediterranean Sea) is considered. For the sake of clarity, a small horizontal shift between the data points for the same frequency has been introduced.

Consequently, the first two parameters of the emissivity vector $(q = 1, 2)$ are expressed by

$$\begin{aligned}\varepsilon_q = {} & \alpha_{0q} + \alpha_{1q} u_{19} + \alpha_{2q} u_{19}^2 + \alpha_{3q} T_s \\ & + \alpha_{4q} T_s^2 + \alpha_{5q} u_{19} \cos\varphi + \alpha_{6q} u_{19}^2 \cos\varphi \\ & + \alpha_{7q} u_{19} \cos 2\varphi + \alpha_{8q} u_{19}^2 \cos 2\varphi. \end{aligned} \tag{13}$$

As for $\varepsilon_{3,4}$, we have adopted the same functional form as that given by Yueh *et al.* [30]. This leads to the following formula for the third and fourth parameters of the emissivity vector $(q = 3, 4)$:

$$\begin{aligned}\varepsilon_q = {} & d_{0q} + \delta_{1q} \{1 - \exp[-(u_{10}/r_1)^{\rho_1}]\} \sin\varphi \\ & + \delta_{2q} \{1 - \exp[-(u_{10}/r_2)^{\rho_2}]\} \sin\varphi \\ & + \delta_{3q} \{1 - \exp[-(u_{10}/r_3)^{\rho_3}]\} \sin 2\varphi \\ & + \delta_{4q} \{1 - \exp[-(u_{10}/r_4)^{\rho_4}]\} \sin 2\varphi \end{aligned} \tag{14}$$

where u_{10} denotes the wind speed at 10 m above sea level. It has been calculated from u_* by using the expression that is given in [4], in which a neutral stability assumption is done, so that the wind speed increases logarithmically with height. For r_i and $\rho_i (i = 1 : 4)$, we have retained the values that are given in [30]. The coefficients $\alpha_{iq} (i = 0 : 8)$ and $\delta_{iq} (i = 0 : 4)$, which are univocally identifying the RMFs, have been derived from a regression analysis of the training set. The RMF-derived simulations, which represent our benchmark, have been produced by applying (11), (13), and (14) to the inputs from the validation data sets.

C. Analysis of the Numerical Results

To statistically analyze the results of the comparisons between NN- and RMF-derived $\mathbf{T}_B$'s with those produced by SEAWIND, we have considered normalized bias error m_e and normalized standard deviation error σ_e. They are obtained by dividing the mean and standard deviation of the error in each element $T_{Bq} (q = 1 : 4)$ of the Stokes' vector by the prior standard deviation of the element itself, as deduced from the validation database. This normalization is made to obtain error parameters of approximately the same order of magnitude, despite of the dynamic range of T_{Bq}.

TABLE II
$m_e \pm \sigma_e$ FOR THE FOUR COMPONENTS OF THE 37-GHz MODIFIED STOKES' VECTOR. DB1 (MEDITERRANEAN SEA) IS CONSIDERED

	T_{Bv}[K]	T_{Bh}[K]	U [K]	V (K)
RMF's	-0.02±0.03	-0.04±0.05	0.00±0.14	0.01±0.09
LMNN	0.02±0.02	0.00±0.03	0.00±0.05	0.01±0.05
BRNN	0.02±0.02	0.01±0.02	0.00±0.04	0.00±0.04

For the validation data set of the Mediterranean Sea (DB1), the results for T_{Bv}, T_{Bh}, U, and V are shown in Fig. 3 in terms of $m_e \pm \sigma_e$ for the three WindSat frequencies. The solid lines identify the interval $[-\sigma_e, +\sigma_e]$ around m_e, while the values of m_e are represented by squares (RMFs), crosses (NN with LM training algorithm), and circles (NN with Bayesian regularized training). It can be noticed that NNs yield normalized biases that are almost equal to 0, whereas RMFs tend to underestimate the first two components of the modified Stokes' vector, particularly, at 18.7 and 37 GHz [see Fig. 3(a) and (b)]. Moreover, the normalized standard deviation errors for U and V that are exhibited by RMFs are much higher than those that are associated with NNs, due to the robustness properties of the latter one. Among the considered training algorithms, Bayesian regularization yields the smallest σ_e, thus reproducing the SEAWIND simulations most accurately.

The values of $m_e \pm \sigma_e$ are reported in Table II. For the sake of conciseness, only the 37-GHz channels are included since they generally present the largest differences with respect to SEAWIND, being more affected by the atmosphere and more sensitive to wind speed. Note that the correlation coefficient

TABLE III
$m_e \pm \sigma_e$ FOR THE FOUR COMPONENTS OF THE 37-GHz MODIFIED STOKES' VECTOR. DB2 (OPEN OCEAN) IS CONSIDERED

	T_{Bv}(K)	T_{Bh}(K)	U (K)	V (K)
RMF's	0.02±0.03	0.01±0.04	0.02±0.20	-0.01±0.12
LMNN	-0.02±0.02	-0.01±0.02	0.00±0.10	0.00±0.09
BRNN	-0.02±0.02	-0.01±0.01	0.00±0.06	0.00±0.05

between SEAWIND and both RMFs and NNs is not reported since it is always close to 1.

DB1 consists of 1000 records. Since a practical rule to ensure a good estimate of an N-dimensional statistics (up to second moments) is to use at least $10 \times N^2$ samples [35], we are an order of magnitude above, being in this case, $N = 1$. It is worth mentioning that, to generate 1000 simulations by means of SEAWIND, it takes about two days (with a personal computer with a Pentium 4 processor), while, once a network is properly trained, the generation of 1000 simulations takes only about 0.03 s by running the NN as a forward model.

To verify the validity of our method also for different climatic conditions, we also have applied NNs and RMFs to DB2 (open ocean). The results are shown in Table III for the 37-GHz channels. In this case too, BRNN yields the best results. This is more evident for σ_e than for m_e, thus confirming that Bayesian regularization training allows the network to generalize better and, consequently, to be more robust.

DB1 and DB2 have been built to validate our approach from a statistical point of view. To show detailed comparisons between SEAWIND and NN outputs, another exercise has been accomplished using BRNN for the 37-GHz channel. We have produced TSM and NN outputs for φ varying from 0° to 360° with a step that is equal to 30°, u_* varying from 0.05 to 0.85 m/s with a step of 0.1 m/s (u_{19} from 1.2 to 18.9 m/s), and for three values of τ (0.06, 0.09, and 0.12). Then, for each τ, the azimuthal Fourier harmonic coefficients of the four components of $\mathbf{T}_B$ have been derived as functions of u_{19} for both SEAWIND and BRNN. Fig. 4 shows the comparison for the three harmonics of $T_{\rm Bv}$ (denoted by $T_{\rm Bv0}$, $T_{\rm Bv1}$, and $T_{\rm Bv2}$) and $T_{\rm Bh}$ ($T_{\rm Bh0}$, $T_{\rm Bh1}$, and $T_{\rm Bh2}$). Fig. 5 provides the analogous comparison (only first and second harmonics, obviously) for U (U_1 and U_2) and V (V_1 and V_2). For the sake of clarity, the plots of the first and second harmonic retain only curves with $\tau = 0.06$ and $\tau = 0.12$, respectively. SEAWIND simulations are denoted by asterisks ($\tau = 0.06$), plus signs ($\tau = 0.09$), and crosses ($\tau = 0.12$). BRNN simulations are represented by solid lines (0.06), dotted lines (0.09), and dashed lines (0.12). These figures demonstrate the capability of the network to reproduce the sensitivity of the physically based polarimetric model that is implemented in SEAWIND to both wind speed and atmospheric transmittance. There is only a slight underestimation (less than 0.5 K) of $T_{\rm Bv1}$ and $T_{\rm Bh1}$ for high wind speeds ($u_{19} > 15$ m/s).

D. Impact on Wind Speed Retrieval

Any forward model is used within the retrieval task either to generate training sets or to run iterative estimation algorithms (e.g., [36]). The final step of our study regards the impact of the discrepancies between SEAWIND and NNs on wind speed

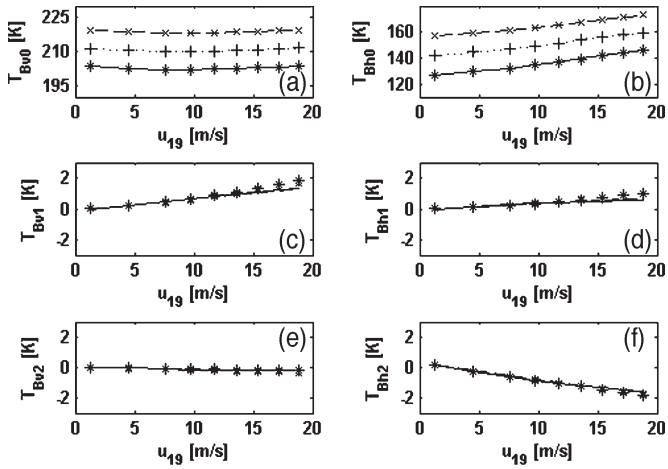

Fig. 4. Azimuthal Fourier harmonic coefficients versus wind speed of 37-GHz SEAWIND and BRNN simulations for (a) T_{Bv0}, (b) T_{Bh0}, (c) T_{Bv1}, (d) T_{Bh1}, (e) T_{Bv2}, and (f) T_{Bh2}. Three optical thicknesses are considered: (SEAWIND: asterisks, BRNN: solid lines) 0.06, (SEAWIND: plus signs, BRNN: dotted lines) 0.09, and (SEAWIND: crosses, BRNN: dashed lines) 0.12.

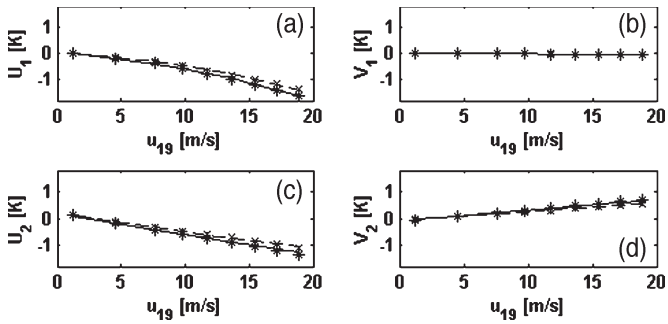

Fig. 5. Azimuthal Fourier harmonic coefficients versus wind speed of 37-GHz SEAWIND and BRNN simulations for (a) U_1, (b) V_1, (c) U_2, and (d) V_2. Two optical thicknesses are considered: (SEAWIND: asterisks, BRNN: solid lines) 0.06 and (SEAWIND: crosses, BRNN: dashed lines) 0.12.

estimations. Having this objective in mind, we have evaluated the effect of building a data set to train a wind-speed estimator using: 1) the SEAWIND physically based forward model and 2) the BRNN approximated forward model.

Since a full implementation of an accurate algorithm for wind vector retrieval is beyond the scope of this paper, to give an estimate of such impact we have adopted a linear regression technique, very often used as a benchmark for estimating wind speed [9], [37]. We have used $T_{\rm Bv}$'s and $T_{\rm Bh}$'s as u_{19} predictors, by assuming a first-degree polynomial relationship

$$u_{19} = p_0 + \sum_{q=1}^{2} \sum_{i=1}^{3} p_{qi} T_{Bq}(f_i) \tag{15}$$

where p_{qi} and p_0 are the coefficients, and $f_i (i = 0, \ldots, 3)$ are the three frequencies that are considered in this paper. We emphasize that this is only a theoretical exercise, and it is understood that an algorithm of practical use should also include 23.8 GHz, to account for the atmospheric water vapor (e.g., [30]).

To develop the two wind-speed estimators based on (15), we have accomplished a systematic sampling [9] to divide DB1

in two subsets (each one including 500 records), which are denoted by DB1′ for training and DB1″ for testing. Then, we have performed a regression analysis to compute two sets of coefficients p_{qi} and p_0, using: 1) the SEAWIND simulations belonging to DB1′ and the corresponding u_{19} and 2) the brightness temperatures that are produced by applying BRNN to DB1′ (and the same u_{19}, obviously).

To evaluate the behavior of these two estimators, they have been applied to the same set of brightness temperatures, i.e., to those belonging to DB1″ that have been simulated by means of SEAWIND, which is considered the "truth" in this exercise. The statistics of the difference between u_{19} that is estimated by the two regressions, based on SEAWIND- and BRNN-derived training sets, have been finally calculated. The mean value and the standard deviation of this difference have been found to be equal to 0.04 and 0.08 m/s, respectively. If a Gaussian noise with 0-K mean and 1-K standard deviation is added to the T_B's belonging to both the training (DB1′) and testing (DB1″) sets, as it is commonly done to increase the estimator robustness, both the mean value and the standard deviation of the u_{19} difference become negligible. In other words, the noise tends to mask the differences between BRNN- and SEAWIND-derived brightness temperatures, and the two estimators become substantially identical.

It is worth mentioning that the root-mean-square difference between u_{19} estimates is much smaller than the error that is expected for wind speed retrievals. For instance, in [9], using the SSM/I radiometer in the Mediterranean Sea (to which DB1 is related), the root-mean-square error has been found on the order of 1.4 m/s. We can therefore foresee a fairly low impact of the errors in the NN TSM emulation on u_{19} estimates.

V. Conclusion

An NN has been proposed for simulating satellite microwave polarimetric observations of the sea surface. This technique has been applied to approximate the behavior of a software package implementing the TSM. The three WindSat fully polarimetric channels have been considered in this study. The use of an NN has considerably improved the computational efficiency of the forward model (two days versus 0.03 s to produce 1000 simulations, for a given frequency).

It has been demonstrated that an NN reproduces the behavior of the TSM fairly well, generally improving the accuracy that is achievable with a standard model function approach. Two NN training algorithms have been taken into consideration, and the Bayesian regularization has yielded the best results due to its generalization characteristic. A preliminary analysis seems to indicate that a retrieval algorithm that is trained by simulations that are produced by an NN provides wind speed estimates that are very similar to those that are supplied by an algorithm that is trained directly by the TSM.

Besides its use within an inversion scheme, an NN approach may be important for validation/calibration of the physically based forward model as well. Although a direct test of the physical model is preferable, the low computational efficiency hampers the generation of large validation sets spanning many different meteorological conditions, as required to ensure a reliable verification. This may suggest the use of the faster NN counterpart, which can rapidly give an indication of the suitability of any upgrade of the physical model.

Finally, further advantage of this approach stems from the opportunity to train the network on a database merging both model outputs and real measurements, thus providing an empirical constraint to the theoretical model.

Acknowledgment

The authors would like to thank the Guest Editor and the reviewers for their useful comments and suggestions, which helped to improve this paper.

References

[1] S. H. Yueh, W. J. Wilson, F. K. Li, S. V. Nghiem, and W. B. Ricketts, "Polarimetric measurements of sea surface brightness temperatures using an aircraft k-band radiometer," *IEEE Trans. Geosci. Remote Sens.*, vol. 33, no. 1, pp. 85–92, Jan. 1995.

[2] S. H. Yueh, W. J. Wilson, S. J. Di Nardo, and F. K. Li, "Polarimetric microwave brightness signatures of ocean wind direction," *IEEE Trans. Geosci. Remote Sens.*, vol. 37, no. 2, pp. 949–959, Mar. 1999.

[3] P. W. Gaiser *et al.*, "The Windsat spaceborne polarimetric microwave radiometer: Sensor description and early orbit performance," *IEEE Trans. Geosci. Remote Sens.*, vol. 42, no. 11, pp. 2347–2361, Nov. 2004.

[4] S. H. Yueh, "Modeling of wind direction signals in polarimetric sea surface brightness temperatures," *IEEE Trans. Geosci. Remote Sens.*, vol. 35, no. 6, pp. 1400–1418, Nov. 1997.

[5] P. Coppo, J. T. Johnson, L. Guerriero, J. A. Kong, G. Macelloni, F. S. Marzano, P. Pampaloni, N. Pierdicca, and Y. Zhang, *Polarimetry for Passive Remote Sensing*, Jun. 1996. Final report ESTEC/Contract AO/1-2917/94/NL/NB.

[6] K. S. Germain, G. A. Poe, and P. W. Gaiser, "Polarimetric emission model of the sea at microwave frequencies and comparison with measurements," *Progress Electrom. Res.*, vol. PIER 37, pp. 1–30, 2002.

[7] P. Pampaloni, L. Guerriero, G. Macelloni, and N. Pierdicca, "'SEAWIND': A physical model for simulating ocean wind measurements by means of radio polarimetry," in *Proc. Int. Workshop POLRAD*, Aug. 1996, pp. 7–18.

[8] N. Pierdicca, F. S. Marzano, L. Guerriero, and P. Pampaloni, "On the effect of atmospheric emission upon the passive microwave polarimetric response of an azimuthally anisotropic sea surface," *Progress Electrom. Res.*, vol. PIER 26, pp. 223–248, 2000.

[9] L. Pulvirenti and N. Pierdicca, "Retrieval of atmospheric and surface parameters from satellite microwave radiometers over the Mediterranean Sea," *IEEE Trans. Geosci. Remote Sens.*, vol. 44, no. 1, pp. 90–101, Jan. 2006.

[10] D. R. Lyzenga and J. F. Vesecky, "Two-scale polarimetric emissivity model: Efficiency improvements and comparisons with data," *Progr. Electromagn. Res.*, vol. 37, pp. 205–219, 2002.

[11] J. T. Johnson, "An efficient two-scale model for the computation of thermal emission and atmospheric reflection from the sea surface," *IEEE Trans.Geosci. Remote Sens.*, vol. 44, no. 3, pp. 549–559, Mar. 2006.

[12] D. R. Lyzenga, "Comparison of Windsat brightness temperatures with two-scale model predictions," *IEEE Trans.Geosci. Remote Sens.*, vol. 44, no. 3, pp. 560–568, Mar. 2006.

[13] K. Hornik, M. Stinchcom, and H. White, "Multi-layered feedforward networks are universal approximators," *Neural Netw.*, vol. 2, no. 5, pp. 359–366, 1989.

[14] V. M. Krasnopolsky, D. V. Chalikov, and H. L. Tolman, "A neural network technique to improve computational efficiency of numerical oceanic models," *Ocean Model.*, vol. 4, no. 3, pp. 363–383, Jun. 2002.

[15] L. Barthes, C. Mallet, and P. Gole, "Neural network model for atmospheric attenuation retrieval between 20 and 50 GHz by means of dual-frequency microwave radiometers," *Radio Sci.*, vol. 38, no. 5, pp. 1082–1100, 2003.

[16] S. H. Yueh, S. V. Nghiem, W. Wilson, F. K. Li, J. T. Johnson, and J. A. Kong, "Polarimetric thermal emission from periodic water surface," *Radio Sci.*, vol. 29, no. 1, pp. 87–96, Jan./Feb. 1994.

[17] J. T. Johnson, J. A. Kong, R. T. Shin, S. H. Yueh, S. V. Nghiem, and R. Kwok, "Polarimetric thermal emission from rough ocean surfaces," *J. Electromagn. Waves Appl.*, vol. 8, no. 1, pp. 43–59, 1994.

[18] W. J. Ellison, A. Balana, G. Delbos, K. Lamkaouchi, L. Eymard, C. Guillou, and C. Prigent, "New permittivity measurements of seawater," *Radio Sci.*, vol. 33, no. 3, pp. 639–648, 1998.
[19] P. C. Pandey and R. K. Kakar, "An empirical microwave emissivity model for a foam-covered sea," *IEEE J. Ocean. Eng.*, vol. 7, no. 3, pp. 135–140, Jul. 1982.
[20] T. T. Wilheit, "A model for the microwave emissivity of the ocean's surface as a function of wind speed," *IEEE Trans. Geosci. Electron.*, vol. 17, no. 4, pp. 244–249, Oct. 1979.
[21] S. L. Durden and J. F. Vesecky, "A physical radar cross-section model for a wind-driven sea with swell," *IEEE J. Ocean. Eng.*, vol. OE-10, no. 4, pp. 445–451, Oct. 1985.
[22] S. Haykin, *Neural Networks: A Comprehensive Foundation*. New York: Mcmillan College, 1995.
[23] E. Sontag, "Feedback stabilization using two-hidden-layer nets," *IEEE Trans. Neural Netw.*, vol. 3, no. 6, pp. 981–990, Nov. 1992.
[24] F. S. Marzano, E. Picciotti, and G. Vulpiani, "Rain field and reflectivity vertical profile reconstruction from *C*-band radar volumetric data," *IEEE Trans. Geosci. Remote Sens.*, vol. 42, no. 4, pp. 1033–1046, 2004.
[25] D. E. Rumelhart, G. E. Hinton, and R. J. Williams, "Learning representations by back-propagating errors," *Nature*, vol. 323, pp. 533–536, 1986.
[26] M. T. Hagan, H. B. Demuth, and M. H. Beale, *Neural Network Design*. Boston, MA: PWS-Kent, 1996.
[27] F. Aires, A. Chédin, N. A. Scott, and W. B. Rossow, "A regularized neural net approach for retrieval of atmospheric and surface temperature with the IASI instrument," *J. Appl. Meteorol.*, vol. 41, no. 2, pp. 144–159, Feb. 2002.
[28] D. J. C. MacKay, "Bayesian interpolation," *Neural Comput.*, vol. 4, no. 3, pp. 415–447, May 1992.
[29] L. Pulvirenti, F. S. Marzano, and N. Pierdicca, "Modeling microwave fully-polarimetric passive observations of sea surface: A neural network approach," in *Proc. MicoRad*, Puerto Rico, Feb. 2006. CD-ROM.
[30] S. H. Yueh, W. J. Wilson, S. J. Dinardo, and S. V. Hsiao, "Polarimetric microwave wind radiometer model function and retrieval testing for WindSat," *IEEE Trans. Geosci. Remote Sens.*, vol. 44, no. 3, pp. 584–596, Mar. 2006.
[31] N. Pierdicca, B. Greco, C. Bignami, P. Ferrazzoli, V. Mattioli, and L. Pulvirenti, "The calibration of the Envisat radar altimeter receiver by a passive technique," *IEEE Trans. Geosci. Remote Sens.*, vol. 44, no. 11, pp. 3297–3307, Nov. 2006.
[32] F. J. Wentz and T. Meissner, *Algorithm Theoretical Basis Document: AMSR Ocean Algorithm, Version 2*. Santa Rosa, CA: Remote Sens. Syst., 1999.
[33] M. H. Bettenhausen, C. K. Smith, R. M. Bevilacqua, N. Wang, P. W. Gaiser, and S. Cox, "A nonlinear optimization algorithm for Windsat wind vector retrievals," *IEEE Trans. Geosci. Remote Sens.*, vol. 44, no. 3, pp. 597–610, Mar. 2006.
[34] S. T. Brown, C. S. Ruf, and D. R. Lyzenga, "An emissivity-based wind vector retrieval algorithm for the Windsat polarimetric radiometer," *IEEE Trans. Geosci. Remote Sens.*, vol. 44, no. 3, pp. 611–621, Mar. 2006.
[35] J. A. Richards and X. Jia, *Remote Sensing Digital Image Analysis: An Introduction*, 4th ed. New York: Springer-Verlag, 2006.
[36] D. T. Davis, Z. Chen, J.-N. Hwang, L. Tsang, and E. Njoku, "Solving inverse problems by Bayesian iterative inversion of a forward model with applications to parameter mapping using SMMR remote sensing data," *IEEE Trans. Geosci. Remote Sens.*, vol. 33, no. 5, pp. 1182–1193, Sep. 1995.
[37] M. A. Goodberlet, C. T. Swift, and J. C. Wilkerson, "Remote sensing of ocean surface winds with the special sensor microwave/imager," *J. Geophys. Res.*, vol. 94, no. C10, pp. 14 547–14 555, Oct. 1989.

Luca Pulvirenti (M'07) received the Laurea degree in electronic engineering and the Ph.D. degree in electromagnetism from the University of Rome "La Sapienza," Rome, Italy, in 1999 and 2004, respectively.

He presently holds a Postdoctoral position in the Department of Electronic Engineering, University of Rome "La Sapienza," teaching a course on electromagnetic propagation. His research interests include microwave remote sensing of the atmosphere and earth's surface, electromagnetic scattering models, and inverse electromagnetic problems.

Dr. Pulvirenti is a member of the Italian Society of in Electromagnetism (SiEM) and Italian Association of Remote Sensing (AIT).

Frank Silvio Marzano (S'89–M'99–SM'03) received the Laurea degree (*cum laude*) in electrical engineering and the Ph.D. degree in applied electromagnetics from the University of Rome "La Sapienza," Rome, Italy, in 1988 and 1993, respectively.

In 1993, he collaborated with the Institute of Atmospheric Physics, Consiglio Nazionale delle Ricerche, Rome. From 1994 to 1996, he was with the Italian Space Agency, Rome, as a Postdoctorate Researcher. After being a Lecturer at the University of Perugia, Perugia, Italy, in 1997, he joined the Department of Electrical Engineering and Cofounded the Center of Excellence CETEMPS, University of L'Aquila, L'Aquila, Italy, where he coordinated the Satellite and Radar Remote Sensing Laboratory. In 2005, he joined the Department of Electronic Engineering, University of Rome "La Sapienza," where he currently teaches courses on antennas and remote sensing. He has published more than 65 papers on international refereed journals and more than 120 extended abstracts in conference proceedings. His current research interests include passive and active remote sensing of the atmosphere from ground-based, airborne, and spaceborne platforms, with a particular focus on precipitation using microwave and infrared data, development of inversion methods, radiative transfer modeling of scattering media, and radar meteorology issues. He is also involved on radiopropagation topics in relation to incoherent wave modeling, scintillation prediction, and rain fading analysis along satellite microwave links.

Dr. Marzano is a member of the Italian Society of Electromagnetics (SiEM). Since 2001, he has been the Italian National Delegate for the European COST actions n.720 on atmospheric profiling by ground-based remote sensing and n.280 on satellite fade mitigation techniques. Since January 2004, he has been acting as an Associated Editor of the IEEE GEOSCIENCE REMOTE SENSING LETTERS. In 2004 and 2006, he was a Co-Guest Editor of the special issues on MicroRad for IEEE TRANSACTIONS ON GEOSCIENCE AND REMOTE SENSING. He was the recipient of the Young Scientist Award of XXIV General Assembly of the International Union of Radio Science (URSI) in 1993 and the Alan Berman Publication Award (ARPAD) from the Naval Research Laboratory, Washington, DC, in 1998.

Nazzareno Pierdicca (M'04) was born in Rome, Italy, on June 11, 1954. He received the Laurea (Ph.D.) degree (*cum laude*) in electronic engineering from the University of Rome "La Sapienza," Rome, Italy, in 1981.

During 1978–1982, he was with the Italian Agency for Alternative Energy (ENEA), performing research and development activities in the field of thermal and mechanical behavior of nuclear fuel rods. From 1982 to 1990, he was with the Remote Sensing Division, Telespazio, Rome. In November 1990, he joined the Department of Electronic Engineering, Faculty of Engineering, University of Rome "La Sapienza," where he is currently an Associate Professor and teaches remote sensing and antennas. He was involved and was responsible in various projects concerning remote sensing applications, data interpretation, and ground segment design. He was a Principal Investigator of the ESA/JRC Agrisar'86 airborne campaign and a Co-Investigator of the X-SAR/SIR-C experiment. He has been an Investigator of the MAC Europe'91 and X-SAR/SIR-C experiments. His research interests include electromagnetic scattering models, microwave radiometry of the atmosphere, and SAR land applications.

Prof. Pierdicca is the Chairman of the Geoscience and Remote Sensing Society (Central Italy Chapter).